Advances in Applied Mathematics and Mechanics
Adv. Appl. Math. Mech., Vol. **7**, No. 5, pp. 569-596

DOI: 10.4208/aamm.2014.m523
October 2015

Numerical Simulations of Unsteady Flows From Rarefied Transition to Continuum Using Gas-Kinetic Unified Algorithm

Junlin Wu[1], Zhihui Li[1,2,*], Aoping Peng[1] and Xinyu Jiang[1]

[1] *Hypervelocity Aerodynamics Institute, China Aerodynamics Research and Development Center, Mianyang 621000, China*
[2] *National Laboratory for Computational Fluid Dynamics, Beijing 100191, China*

Received 1 March 2014; Accepted (in revised version) 5 November 2014

Abstract. Numerical simulations of unsteady gas flows are studied on the basis of Gas-Kinetic Unified Algorithm (GKUA) from rarefied transition to continuum flow regimes. Several typical examples are adopted. An unsteady flow solver is developed by solving the Boltzmann model equations, including the Shakhov model and the Rykov model etc. The Rykov kinetic equation involving the effect of rotational energy can be transformed into two kinetic governing equations with inelastic and elastic collisions by integrating the molecular velocity distribution function with the weight factor on the energy of rotational motion. Then, the reduced velocity distribution functions are devised to further simplify the governing equation for one- and two-dimensional flows. The simultaneous equations are numerically solved by the discrete velocity ordinate (DVO) method in velocity space and the finite-difference schemes in physical space. The time-explicit operator-splitting scheme is constructed, and numerical stability conditions to ascertain the time step are discussed. As the application of the newly developed GKUA, several unsteady varying processes of one- and two-dimensional flows with different Knudsen number are simulated, and the unsteady transport phenomena and rarefied effects are revealed and analyzed. It is validated that the GKUA solver is competent for simulations of unsteady gas dynamics covering various flow regimes.

AMS subject classifications: 82C40, 74H15

Key words: Unsteady flow, covering various flow regimes, kinetic theory of gases, Boltzmann model equation, gas-kinetic unified algorithm, discrete velocity ordinate method, Shakov kinetic model, Rykov kinetic model.

*Corresponding author.
Email: zhli0097@x263.net (Z. H. Li)

 ©2015 Global Science Press

https://doi.org/10.4208/aamm.2014.m523 Published online by Cambridge University Press

1 Introduction

How to simulate unsteady aerodynamics covering various flow regimes has been being a difficult and meaningful topic. Studies on unsteady aerodynamics started around 1920 when theoretical analysis became as the primary researching means [1, 2]. From then on, theoretical studies on unsteady flow have been high-speedily developed [3, 4]. At the same time, the improvements of experimental technologies and combination with theoretical researches have been promoted greatly [5–7]. Computational Fluid Dynamics has become of epochal significance to aerodynamics along with the occurrence of Computer. Then, numerical simulations of unsteady problems [8–11] have been developed from inviscid Euler equation to viscid Navier-Stokes equation, from fixed cell to moving mesh, and from fixed aerofoil to swing wing, and different numerical schemes and computational techniques have been advanced.

On the other hand, researches of unsteady flow problems in rarefied transitional flow regimes have arisen to be a popular subject in recent years [12,13]. It is difficult for classical macro-hydrodynamic equations to describe gas flows in such regimes. Consequently, the numerical methods for unsteady flows of rarefied gases need to be developed [14]. The most widely used one is the direct simulation Monte Carlo (DSMC) method [15] proposed by Bird as early as 1963. The DSMC method represents the massive real gas molecules by a finite set of simulated particles. The spatial coordinates, velocity components and internal energies of these simulated molecules are stored in the computers, and their values change with time because of the movement of simulated molecules, the interactions with the boundary and the collisions between simulated molecules. It eventually achieves the simulation of real gas flow by the statistics of the states of motion from the simulated molecules within the cell. With the developments during the past decades, the DSMC method has been widely applied and validated by rarefied gas dynamics including unsteady flow problems [16–20]. Recently, the DSMC method is adopted for a transient rarefied gas flow through a short tube [21]. A wide range of gas rarefaction is considered, and some important conclusions are given. The results show that it is complicated and difficult to reveal the transient flow phenomena of rarefied gas. Besides, the DSMC method is used to predict the steady and unsteady rarefied gas flows induced by a rotor-stator interaction in a single-stage disk-type drag pump [22]. Actually, statistical noise and fluctuation caused by probabilistic nature of the DSMC is a disadvantageous influence for unsteady flow simulation [23, 24].

On the basis of mesoscopic Boltzmann-type velocity distribution function theory connecting macroscopic fluid dynamics and microscopic molecular dynamics [25–27], a new class of methods such as the Discrete Velocity Models (DVM) [27, 28, 61], the Lattice Boltzmann Equation (LBE) [29–32] and the Gas-Kinetic Scheme (GKS) [12, 27, 33–36] has been being developed for simulation of gas flows covering various regimes. Although these methods are sometimes designed for macroscopic hydrodynamics [31], they are not based upon macroscopic fluid equations like the Navier-Stokes equations; instead, they are closely related to the kinetic theory or the Boltzmann-BGK-type equation. As

https://doi.org/10.4208/aamm.2014.m523 Published online by Cambridge University Press

notable example, the Lattice Boltzmann method (LBM) has emerged and developed [29–32, 37–39] as a new and effective numerical technique of CFD in the last three decades or so. The LBM based on the two-dimensional nine-velocity model has been developed to numerically simulate unsteady cavity flow for computational aeroacoustic study [32]. It is shown that the LBM could be useful for aeroacoustic computations of low subsonic flows. However, it seems to be difficult for the LBM to obey H-theorem automatically [29] and depict physical phenomenon correctly for high-speed flows. Many studies of unsteady flows are concentrating on the deterministic Boltzmann equation or its model equations [27,35,40–47]. The unsteady problems should be solved on the basis of numerical solutions of the kinetic model equations. Cai [48,49] concentrate their attentions on unsteady high-speed collisionless planar or round jet flows in a vacuum, including the startup, steady and shutting down processes, with the analytical methods based on a set of gas-kinetic solutions. Good applications can be found in studying transient plume flows from space propulsion devices. These analytical exact solutions, however, are limited to some special physical problems in which molecular collisions are neglected with the collisionless Boltzmann equation. Recently, Polikarpov and Graur [47] simulate a transient gas flow through a rectangular slit on the basis of unsteady S-model kinetic equation. It is shown that the time of steady flow establishment depends on the pressure ratio between the tanks and on the gas rarefaction. John and Dimitris [45] investigate the starting gas flow in a cylindrical channel by numerically solving the time dependent Bhatnagar-Gross-Krook (BGK) kinetic equation. Sruti and Alina [46] develop a 3D unsteady rarefied flow solver based on Boltzmann-ESBGK model kinetic equation.

The discrete velocity ordinate (DVO) method is developed and adopted in velocity space, while finite difference schemes are introduced in physical space. On this basis, Li [35,43,50,51] presents the gas-kinetic unified algorithm (GKUA) from rarefied transition to continuum by solving the Boltzmann model equations. The GKUA modifies the Boltzmann-BGK model in two aspects including the local equilibrium distribution function and the molecular collision relaxation parameter, and the resultant Boltzmann model equation links the macroscopic flow variables, gas viscosity transport properties, thermodynamic effect, the flow state parameter and molecular interaction rule with molecular models in unified expressions for the full spectrum of flow regimes. The GKUA has been validated and applied to many steady flows [52,53] around aircrafts and microchannels covering various flow regimes. The kinetic model equation used in GKUA may be BGK, ESBGK or S-model [40–42]. Actually, the solution process of GKUA is to get final steady state by a long-time transition of unsteady simulations. The aim of this paper is to extend the GKUA to analyze the unsteady processes of several representative flows from continuum to highly rarefied flow, which the improved model based on the Boltzmann-Rykov kinetic equation is developed with reduced velocity distribution functions for unsteady flows. This is the first attempt to develop and use the direct Boltzmann gas-kinetic solver to study unsteady gas dynamics covering flow regimes. Time-explicit scheme is developed to simulate the transient flows, and the numerical stability condition to ascertain time-step is discussed for unsteady simulation. The unsteady flows including the one-

https://doi.org/10.4208/aamm.2014.m523 Published online by Cambridge University Press

dimensional shock-tube, the planar jet flow and the gas flow through a slit are studied by solving the S-model [42] equation for monatomic gas flows and the Boltzmann-Rykov model [54] equation involving the effect of rotational degrees of freedom for diatomic gas.

2 Numerical simulation algorithm

Various kinetic model equations can be solved by the GKUA. Therefore, the S-model for monatomic ideal gases and the R-model for diatomic gases involving the effect of rotational degrees of freedom, are adopted to validate and analyze transient gas flows covering various flow regimes.

2.1 S-model equation for ideal gases

Based on an approximation of the Boltzmann equation for pseudo-Maxwellian molecules using the method suggested by [55], Shakhov proposes a technique for constructing a sequence of model equations which provide the correct Prandtl number [42]. The kinetic model of the incomplete third-order approximation has the form

$$\frac{\partial f}{\partial t}+\xi_i\frac{\partial f}{\partial x_i}=v(f^N-f), \tag{2.1a}$$

$$v=\frac{nkT}{\mu},\quad f^N=n\Big(\frac{m}{2\pi kT}\Big)^{3/2}\exp\Big(-\frac{mc^2}{2kT}\Big)\Big[1+(1-\mathrm{Pr})\bar{c}\cdot\bar{q}\Big(\frac{c^2}{RT}-5\Big)\Big/5pRT\Big]. \tag{2.1b}$$

Where $f=f(t,\vec{r},\vec{\xi})$ is a non-negative velocity distribution function, subscript i represents direction of spatial ordinate. v is the collision frequency which can be expressed in terms of macroscopic parameters and molecular interaction models [35,43,50]. μ is the viscosity coefficient, ξ_i is the molecular velocity. n, T, P denote number density, temperature, pressure, respectively. k is the Boltzmann constant, and m is molecular mass. Pr denotes Prandtl number, and $c_i=\xi_i-U_i$. $\bar{q}$ is the heat flux vector. R is the gas constant $R=k/m$.

2.2 R-model equation involving the effect of rotational energy

The relaxation properties of rotational degrees of freedom are analyzed, and moment of inertia is used to describe molecular rotational state. With angular momentum as a collision invariant, Rykov model is proposed in [54,56,57]. The R-model kinetic equation of molecular velocity distribution function is

$$\frac{\partial f}{\partial t}+\xi_i\cdot\frac{\partial f}{\partial x_i}=v_r(f^r-f)+v_t(f^t-f), \tag{2.2a}$$

$$v_r=\frac{P_t}{\mu_t}\cdot\frac{1}{Z},\qquad v_t=\frac{P_t}{\mu_t}\cdot\Big(1-\frac{1}{Z}\Big), \tag{2.2b}$$

https://doi.org/10.4208/aamm.2014.m523 Published online by Cambridge University Press

$$f^t = N(e)\Big(\frac{m}{2\pi kT_t}\Big)^{3/2}\exp\Big(-\frac{mc^2}{2kT_t}\Big)\Big[1-\frac{2}{15}\frac{q_i^t}{nkT_t}\cdot\frac{mc_i}{kT_t}\Big(\frac{5}{2}-\frac{mc^2}{2kT_t}\Big) -(1-\delta)\frac{q_i^r mc_i}{kT_t}\cdot\frac{(\varepsilon-e)}{\theta}\Big], \tag{2.2c}$$

$$f^r = n\Big(\frac{m}{2\pi kT}\Big)^{3/2}\exp\Big(-\frac{mc^2}{2kT}\Big)(kT)^{-1}\exp\Big(-\frac{e}{kT}\Big)\Big[1-\alpha\frac{q_i^t}{P}\cdot\frac{mc_i}{kT}\Big(\frac{5}{2}-\frac{mc^2}{2kT}\Big) -\beta\frac{q_i^r mc_i}{PkT}\cdot\Big(1-\frac{e}{kT}\Big)\Big]. \tag{2.2d}$$

Here $f=f(t,\vec{r},\vec{\xi},e)$, subscripts t and r in Eq. (2.2) denote elastic and inelastic collision respectively. For examples, v_t and v_r are the elastic and inelastic collision frequencies. Z is the inelastic collision relaxation factor, while e is molecular rotational energy. α, β are constants correlative to gas identity. D is self-diffuse coefficient. δ is a constant related to molecular interaction.

This R-model equation can be further simplified by integrating the distribution function over the variable e, and distribution functions f_0 and f_1 are introduced

$$f_0(t,\vec{r},\vec{\xi})=\int f de, \quad f_1(t,\vec{r},\vec{\xi})=\int e f de. \tag{2.3}$$

Sequentially, multiplying Eq. (2.2) by 1 and e, and integrating over the variable e, a closed system for f_0 and f_1 is obtained

$$\begin{cases} \dfrac{\partial f_0}{\partial t}+\xi_i\cdot\dfrac{\partial f_0}{\partial x_i}=v_r({f_0}^r-f_0)+v_t({f_0}^t-f_0), \\ \dfrac{\partial f_1}{\partial t}+\xi_i\cdot\dfrac{\partial f_1}{\partial x_i}=v_r({f_1}^r-f_1)+v_t({f_1}^t-f_1), \end{cases} \tag{2.4a}$$

$$v_r=\frac{P_t}{\mu_t}\cdot\frac{1}{Z}, \qquad v_t=\frac{P_t}{\mu_t}\cdot\Big(1-\frac{1}{Z}\Big), \tag{2.4b}$$

$$f_0^r = n\Big(\frac{m}{2\pi kT}\Big)^{3/2}\exp\Big(-\frac{mc^2}{2kT}\Big)\Big[1-\frac{2}{15}\omega_0\cdot\frac{q_i^t}{P}\cdot\frac{mc_i}{kT}\Big(\frac{5}{2}-\frac{mc^2}{2kT}\Big)\Big], \tag{2.4c}$$

$$f_0^t = n\Big(\frac{m}{2\pi kT_t}\Big)^{3/2}\exp\Big(-\frac{mc^2}{2kT_t}\Big)\Big[1-\frac{2}{15}\cdot\frac{q_i^t}{P_t}\cdot\frac{mc_i}{kT_t}\Big(\frac{5}{2}-\frac{mc^2}{2kT_t}\Big)\Big], \tag{2.4d}$$

$$f_1^r = kTn\Big(\frac{m}{2\pi kT}\Big)^{3/2}\exp\Big(-\frac{mc^2}{2kT}\Big)\Big[1-\frac{2}{15}\omega_0\cdot\frac{q_i^t}{P}\cdot\frac{mc_i}{kT}\Big(\frac{5}{2}-\frac{mc^2}{2kT}\Big)+\omega_1(1-\delta)\frac{q_i^r mc_i}{PkT}\Big], \tag{2.4e}$$

$$f_1^t = \varepsilon n\Big(\frac{m}{2\pi kT_t}\Big)^{3/2}\exp\Big(-\frac{mc^2}{2kT_t}\Big)\Big[1-\frac{2}{15}\cdot\frac{q_i^t}{P_t}\cdot\frac{mc_i}{kT_t}\Big(\frac{5}{2}-\frac{mc^2}{2kT_t}\Big)+(1-\delta)\frac{q_i^r mc_i}{\varepsilon nkT_t}\Big]. \tag{2.4f}$$

The macroscopic gas parameters are expressed in terms of f_0 and f_1 by formulas [35, 54] as follows:

$$n=\int f_0 d\xi, \quad nU_i=\int \xi_i f_0 d\xi, \quad \frac{3}{2}kT_t=\frac{1}{n}\int\frac{mc^2}{2}f_0 d\xi, \tag{2.5a}$$

https://doi.org/10.4208/aamm.2014.m523 Published online by Cambridge University Press

$$q_i^t=\int c_i\frac{mc^2}{2}f_0d\xi,\quad \varepsilon=\frac{1}{n}\int f_1d\xi,\quad q_i^r=\int c_if_1d\xi, \tag{2.5b}$$

$$\frac{5}{2}kT=\frac{3}{2}kT_t+\varepsilon,\quad kT_r=\varepsilon,\quad P_t=nkT_t,\quad P=nkT. \tag{2.5c}$$

Viscosity coefficient μ and inelastic collision relaxation factor Z are specified [56,57] as

$$\mu_t=\mu(T_t)=\mu(T_*)t^{2/3}\mu(T_*)t^{2/3}/\phi(t),\qquad t=T_t/T_*, \tag{2.6a}$$

$$\phi(t)=0.767+0.233t^{-1/6}\exp[-1.17(t-1)], \tag{2.6b}$$

$$Z(T_t,T_r)=\frac{3}{4}\pi\frac{\phi(t)}{t^{1/6}}\frac{9t}{t+8}\left(\frac{T_r}{T_t}\right)\left[0.461+0.5581\left(\frac{T_r}{T_t}\right)+0.0358\left(\frac{T_r}{T_t}\right)^2\right]. \tag{2.6c}$$

For nitrogen, $T_*=91.5K$, $1/\delta=1.55$.

2.3 Non-dimensionalization for the model equations

The Boltzmann gas-kinetic solver of the GKUA is adopted to directly capture the time evolution of the velocity distribution functions for both S-model and R-model. In terms of the GKUA, the non-dimensionalized procedure of variables and equations is needed to unify the same scale of both the microscopic statistical distribution and the macroscopic variables of gas flow in practical computation.

The gas kinetic characteristic variables [35,50–53] are introduced to be referenced values of spatial coordinate, time, number density, flow velocity, temperature, viscosity

$$L,\quad L/\sqrt{2RT_\infty},\quad n_\infty,\quad \sqrt{2RT_\infty},\quad T_\infty,\quad \frac{5}{16}mn_\infty\sqrt{2\pi RT_\infty}\lambda_\infty.$$

Simultaneity, the reference parameters of energy fluxes and distribution functions f_0 and f_1 are

$$mn_\infty(2RT_\infty)^{3/2},\quad n_\infty(2RT_\infty)^{-3/2},\quad mn_\infty RT_\infty(2RT_\infty)^{-3/2}.$$

Here λ_∞ is the mean free path of unperturbed gas, and the most probable thermal velocity $C_{m\infty}$ is the characteristic velocity, $C_{m\infty}=\sqrt{2RT_\infty}$.

The dimensionless model equations can be solved by the DVO method [35, 50, 53], corresponding numerical integral techniques and finite-difference schemes of CFD. It is noticed that the reduced velocity distribution functions can be introduced to further simplify the dimensionless model equations before applying the DVO techniques, which can abate the demand of computer memories and improve calculating efficiency. Taking the two-dimensional R-model (in $x-y$ plane) for example, with dimensionless symbol elided, we define

$$g_1=\int_{-\infty}^{+\infty}f_0d\xi_z,\qquad g_2=\int_{-\infty}^{+\infty}\xi_z^2f_0d\xi_z,\qquad g_3=\int_{-\infty}^{+\infty}f_1d\xi_z. \tag{2.7}$$

https://doi.org/10.4208/aamm.2014.m523 Published online by Cambridge University Press

Substituting Eq. (2.7) into the dimensionless form of Eq. (2.4), we obtain simultaneous equations about reduced velocity distribution functions $g_1(t,x,y,\xi_x,\xi_y)$, $g_2(t,x,y,\xi_x,\xi_y)$, $g_3(t,x,y,\xi_x,\xi_y)$.

$$\begin{cases} \dfrac{\partial g_1}{\partial t}+\xi_x\cdot\dfrac{\partial g_1}{\partial x}+\xi_y\cdot\dfrac{\partial g_1}{\partial y}=v_r(g_1^r-g_1)+v_t(g_1^t-g_1), \\ \dfrac{\partial g_2}{\partial t}+\xi_x\cdot\dfrac{\partial g_2}{\partial x}+\xi_y\cdot\dfrac{\partial g_2}{\partial y}=v_r(g_2^r-g_2)+v_t(g_2^t-g_2), \\ \dfrac{\partial g_3}{\partial t}+\xi_x\cdot\dfrac{\partial g_3}{\partial x}+\xi_y\cdot\dfrac{\partial g_3}{\partial y}=v_r(g_3^r-g_3)+v_t(g_3^t-g_3), \end{cases} \tag{2.8}$$

where

$$\begin{aligned} &g_M(T)=\int f_M(T)d\xi_z=\frac{n}{\pi T}\exp\Big(-\frac{c_x^2+c_y^2}{T}\Big), \\ &g_1^r=g_M(T)\Big[1+\frac{8}{15}\omega_0\cdot\frac{q_x^tc_x+q_y^tc_y}{PT}\cdot\Big(\frac{c_x^2+c_y^2}{T}-2\Big)\Big], \\ &g_2^r=\frac{T}{2}g_M(T)\Big[1+\frac{8}{15}\omega_0\cdot\frac{q_x^tc_x+q_y^tc_y}{PT}\cdot\Big(\frac{c_x^2+c_y^2}{T}-1\Big)\Big], \\ &g_3^r=T\Big[g_1^r+4\omega_1(1-\delta)\cdot g_M(T)\frac{q_x^rc_x+q_y^rc_y}{PT}\Big], \\ &g_1^t=g_M(T_t)\Big[1+\frac{8}{15}\cdot\frac{q_x^tc_x+q_y^tc_y}{P_tT_t}\cdot\Big(\frac{c_x^2+c_y^2}{T_t}-2\Big)\Big], \\ &g_2^t=\frac{T_t}{2}g_M(T_t)\Big[1+\frac{8}{15}\cdot\frac{q_x^tc_x+q_y^tc_y}{P_tT_t}\cdot\Big(\frac{c_x^2+c_y^2}{T_t}-1\Big)\Big], \\ &g_3^t=T_r\Big[g_1^t+4(1-\delta)\cdot g_M(T_t)\frac{q_x^rc_x+q_y^rc_y}{P_tT_r}\Big]. \end{aligned}$$

The dimensionless macroscopic flow parameters are obtained as

$$n=\iint g_1d\xi_xd\xi_y, \qquad nU_i=\iint \xi_ig_1d\xi_xd\xi_y, \tag{2.9a}$$

$$\frac{3}{2}nT_t+nU^2=\iint[(\xi_x^2+\xi_y^2)g_1+g_2]d\xi_xd\xi_y, \qquad nT_r=\iint g_3d\xi_xd\xi_y, \tag{2.9b}$$

$$q_i^t=\iint c_i\Big(\frac{c_x^2+c_y^2}{2}g_1+\frac{1}{2}g_2\Big)d\xi_xd\xi_y, \qquad 2q_i^r=\iint c_ig_3d\xi_xd\xi_y, \tag{2.9c}$$

$$\frac{5}{2}T=\frac{3}{2}T_t+T_r,\quad P_t=nT_t, \qquad P=nT,\quad q_i=q_i^t+q_i^r. \tag{2.9d}$$

Then the DVO method is introduced to numerically discretize the velocity components ξ_x and ξ_y. The DVO points are selected based upon the moment integrals of discrete velocity distribution functions, and then macroscopic flow variables can be obtained by

https://doi.org/10.4208/aamm.2014.m523 Published online by Cambridge University Press

the appropriate discrete velocity quadrature formula in terms of Eq. (2.9) at any time in each point of the physical space.

According to the GKUA, the Eq. (2.8) can be switched from (x,y) in physical space into (ξ,η) in computed coordinate plane [35,50,51] by applying the DVO method

$$\frac{\partial U}{\partial t}+\frac{\partial F}{\partial \zeta}+\frac{\partial E}{\partial \eta}=S. \tag{2.10}$$

Here, $U=J[g_{1\sigma,\delta},\ g_{2\sigma,\delta},\ g_{3\sigma,\delta}]^T$, $F=\bar{U}\cdot U$, $E=\bar{V}\cdot U$, $S=J\bar{S}$; $g_{1\sigma,\delta}=g_{1\sigma,\delta}(t,x,y)$, $g_{2\sigma,\delta}=g_{2\sigma,\delta}(t,x,y)$, $g_{3\sigma,\delta}=g_{3\sigma,\delta}(t,x,y)$, $\sigma=0,1,2,\cdots,2N_2$, $\delta=0,1,2,\cdots,2N_2$, $c_{x\sigma}=\xi_{x\sigma}-U$, $c_{y\sigma}=\xi_{y\sigma}-V$, J is the Jacobian of the general transformation, that is $J=\partial(x,y)/\partial(\xi,\eta)$.

2.4 Time-explicit finite difference scheme

In order to numerically simulate unsteady flows, difference schemes must satisfy dissipation, dispersion and shock control conditions to ensure stability and no mendacious fluctuation, and well capture shockwave and other discontinuities [58]. Besides, the numerical scheme on the boundary should be harmonized with that on central points. The fixed time-step is usually used to explicitly iterate and advance in computation, but this time-step must meet stability requirement. The non-oscillatory, containing no free parameters and dissipative difference (NND) scheme is introduced to discretize the convective terms of spatial coordinates, which possesses high resolving power in capturing shockwave and expansion-wave [59]. The gas-kinetic finite-difference scheme is applied [35,51] by the aid of the unsteady time-splitting technique to numerically solve the reduced velocity distribution functions at each of DVO point [35,61–64]

$$U^{n+1}=L_s(\Delta t/2)L_\eta(\Delta t/2)L_\zeta(\Delta t)L_\eta(\Delta t/2)L_s(\Delta t/2)U^n. \tag{2.11}$$

Here, subscript s indicates source item, ξ, η are ordinates in the computational plane, respectively. The Eq. (2.11) shows that distribution function values after Δt are obtained by iterating two times with half time-step $(\Delta t/2)$ each one time. In this way, time precision of this scheme could be improved.

Every term of Eq. (2.11) is corresponding to numerical computation of non-linear equations, where L_s, L_ξ and L_η denote the difference operators of the colliding relaxation source term and convective movement equations in the two different directions, respectively

$$\frac{\partial U}{\partial t}+\frac{\partial F}{\partial \zeta}=0,\quad \frac{\partial U}{\partial t}+\frac{\partial E}{\partial \eta}=0,\quad \frac{\partial U}{\partial t}=S. \tag{2.12}$$

Finite difference schemes, such as NND-3 and NND-4, are introduced to scan in mathe-

https://doi.org/10.4208/aamm.2014.m523 Published online by Cambridge University Press

matic plane

$$\begin{cases} u_j^{\overline{n+1}} = u_j^n - \dfrac{1}{2}\dfrac{\Delta t}{\Delta s}(h_{j+1/2}^n - h_{j-1/2}^n), \\ u_j^{n+1} = u_j^n - \dfrac{\Delta t}{\Delta s}(h_{j+1/2}^{\overline{n+1}} - h_{j-1/2}^{\overline{n+1}}), \end{cases} \tag{2.13a}$$

$$\begin{cases} u_j^{\overline{n+1}} = u_j^n - \dfrac{\Delta t}{\Delta s}(h_{j+1/2}^n - h_{j-1/2}^n), \\ u_j^{n+1} = \dfrac{1}{2}\Big(u_j^n + u_j^{\overline{n+1}} - \dfrac{\Delta t}{\Delta s}(h_{j+1/2}^{\overline{n+1}} - h_{j-1/2}^{\overline{n+1}})\Big). \end{cases} \tag{2.13b}$$

Here, Eq. (2.13a) and Eq. (2.13b) are corresponding to the NND-3 and NND-4(a) [59], respectively. Both of them are two-order schemes

$$h_{j+\frac{1}{2}} = f_{L,j+\frac{1}{2}} + f_{R,j+\frac{1}{2}}, \tag{2.14a}$$

$$f_{L,j+\frac{1}{2}} = f_j^+ + \frac{1}{2}\text{min mod}\,(\Delta f_{j+\frac{1}{2}}^+, \Delta f_{j-\frac{1}{2}}^+), \tag{2.14b}$$

$$f_{R,j+\frac{1}{2}} = f_{j+1}^- - \frac{1}{2}\text{min mod}\,(\Delta f_{j+\frac{1}{2}}^-, \Delta f_{j+\frac{3}{2}}^-). \tag{2.14c}$$

2.5 Improvement on stability condition of the GKUA

In the former theory of GKUA, the time step Δt in the computation is determined by using both the scheme stability condition Δt_s and mean collision time Δt_c as the first experiment [50–53], where the Δt_s is derived from the finite difference scheme, while the Δt_c is from physical analysis of molecular collisions in DSMC method

$$\Delta t_s = 1 \Big/ \max\Big(\frac{v_r + v_t}{2}, \frac{|\bar{U}|}{\Delta\zeta}, \frac{|\bar{V}|}{\Delta\eta}\Big), \tag{2.15a}$$

$$\Delta t_c = \frac{1}{(v_r + v_t)}\max, \tag{2.15b}$$

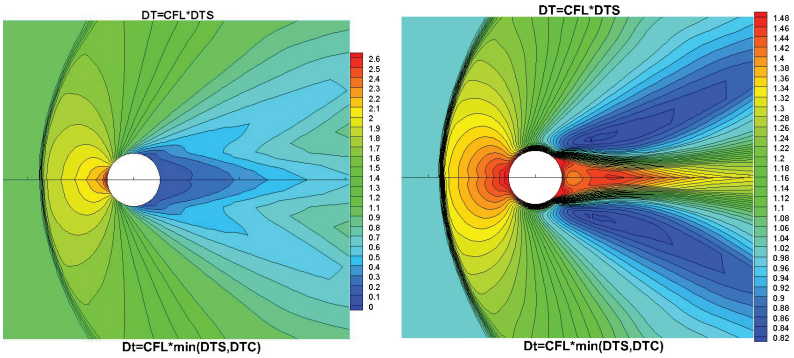
$$\Delta t = CFL \cdot \min(\Delta t_s, \Delta t_c). \tag{2.15c}$$

Here, CFL is the accommodation coefficient for the time step, and $CFL \leq 1$.

The GKUA is a deterministic gas-kinetic solver by directly solving the Boltzmann model equation, in which the scheme stability condition should be satisfied. However, the DSMC is a probabilistic statistics method, which is much different from the GKUA. The restricting condition of the mean collision time Δt_c can be removed from the stability condition Eq. (2.15c) of the GKUA. Recently, Li and Fang etc. [60] investigate the convergence proof of the DSMC method and the GKUA for the Boltzmann equation, and it is validated that the time step in the GKUA can be determined only by the scheme stability condition Δt_s.

In practical computation, when flows with small Kn numbers are in continuum or near-continuum regimes, Δt_c may lead to smaller time step and slower convergence rate.

https://doi.org/10.4208/aamm.2014.m523 Published online by Cambridge University Press



(a) Density (b) Temperature

Figure 1: Non-dimensional density and temperature contours for $Kn=0.0005$ for steady flows past a cylinder with different time steps.

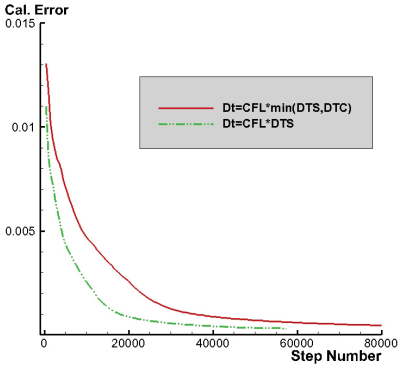


Figure 2: Convergence curves for flows past a cylinder with different time steps.

A two-dimensional steady flow past a cylinder is taken for example, in which the free-stream Mach number is 1.6. Two stability conditions with Δt_c and without Δt_c are taken into account for numerical computation of the cylinder flow. Non-dimensional density and temperature contours for $Kn=0.0005$ are given in Fig. 1, in which $\Delta t_c=2.08\times10^{-4}$ and $\Delta t_s=4.15\times10^{-4}$, respectively. It is shown that the computed contours and flow structures are completely identical with these two different time steps, where the upper part denotes the computed results corresponding to $\Delta t=CFL\Delta t_s$ and the lower part denotes the computed results corresponding to Eq. (2.15c). Then, Fig. 2 shows the convergence curves of these computing processes. It is shown that convergence rate without the consideration of Δt_c is obviously faster. Consequently, harsher time step is dispensable to concrete computation.

For flows with bigger Kn numbers in rarefied transitional regime, generally, $\Delta t_c \geq \Delta t_s$. Thus the mean collision time Δt_c will automatically meet if the scheme stability condition Δt_s is satisfied. For example, $\Delta t_c=2.93\times10^{-3}$ and $\Delta t_s=1.26\times10^{-3}$ in the flow past a cylinder when $Kn=0.01$.

https://doi.org/10.4208/aamm.2014.m523 Published online by Cambridge University Press

In a word, only the scheme stability condition Δt_s is used as time-step criterion for unsteady flow

$$\Delta t = CFL \Big/ \max\Big(\frac{v_r+v_t}{2}, \frac{|\bar{U}|}{\Delta\zeta}, \frac{|\bar{V}|}{\Delta\eta}\Big). \tag{2.16}$$

3 Numerical results and analysis

In this section, the newly developed GKUA will be used to solve the one- and two-dimensional unsteady flows covering various flow regimes including the unsteady shock-tube flow, the two-dimensional flow through a slit, the planar jet flow and the interaction of a normal shock with detached shock around a circular cylinder.

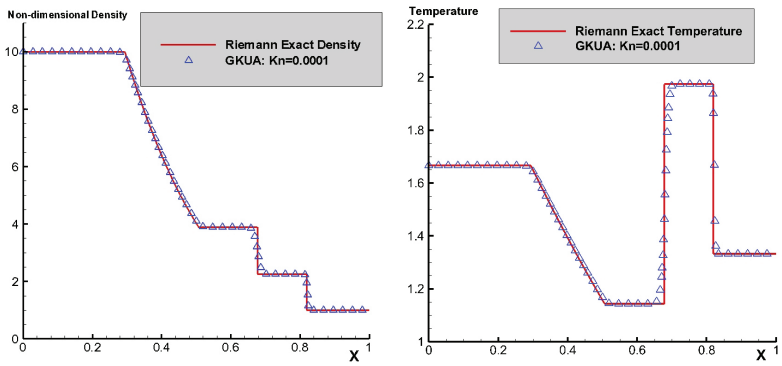
3.1 Simulation of one-dimensional unsteady shock-tube problems with the range of $0.0001 \le K_n \le 1$

In the interval of $(0,1)$, a diaphragm is located at $x=0.5$ so that the whole interval is divided into two parts with different initial states. The diaphragm is instantaneously taken away at $t=0$.

$0 \le x \le 0.5$	$0.5 \le x \le 1$

Non-dimensional macroscopic parameters in this shock-tube are initially set $\rho=10.0$, $T=1.667$, $U=0.0$, when $0 \le x \le 0.5$. $\rho=1.0$, $T=1.333$, $U=0.0$ when $0.5 \le x \le 1$.

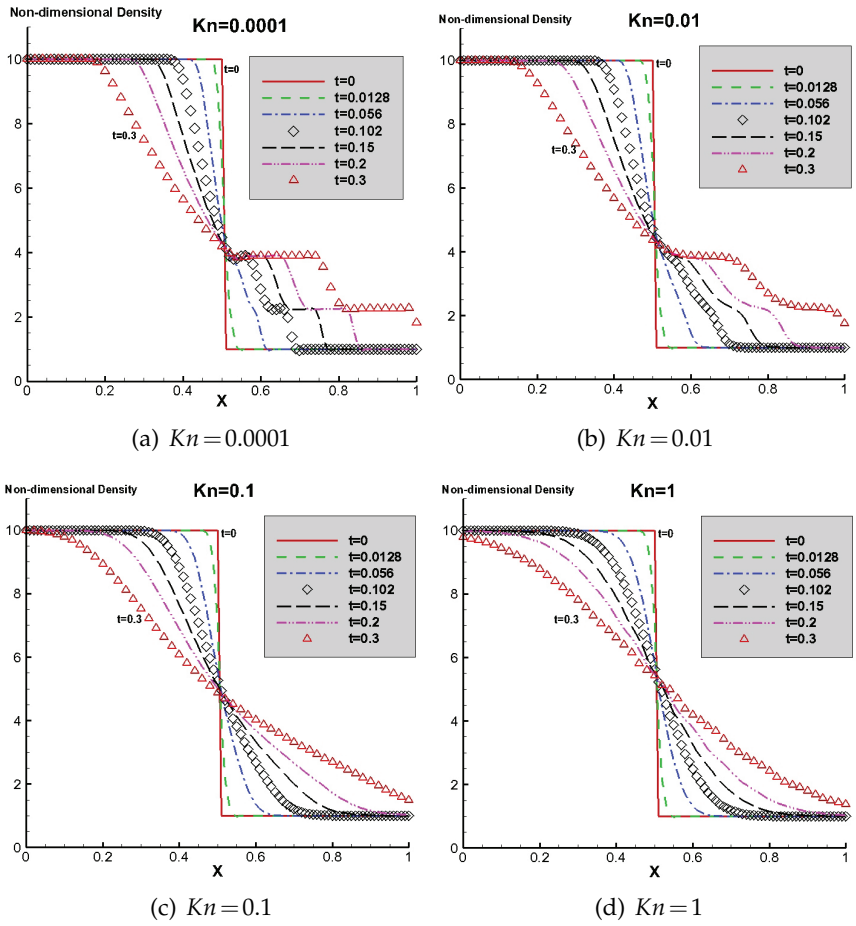
The flow gas is nitrogen with specific heat ratio $\gamma=1.4$ and the Knudsen (Kn) number is gradually decreased from $Kn=1$ to $Kn=0.0001$. The newly developed GKUA is applied to compute this shock-tube flow by the use of the R-model, where the rotational characteristic parameter is set as $B=0.34$ $(B=T_\infty/T_*)$. Fig. 3 shows the computed profiles (symbols Δ) of density and temperature for $Kn=0.0001$, which are compared with



(a) Density (b) Temperature

Figure 3: Comparison of computed shock-tube profiles for $Kn=0.0001$ with Riemann solutions in continuum regime at $t=0.1912$.

https://doi.org/10.4208/aamm.2014.m523 Published online by Cambridge University Press



(a) $Kn=0.0001$ (b) $Kn=0.01$

(c) $Kn=0.1$ (d) $Kn=1$

Figure 4: Comparison of computed shock-tube profiles for $Kn=0.0001$ with Riemann solutions in continuum regime at $t=0.1912$.

the Riemann exact results of inviscid gas dynamics in continuum flow regime at the time $t=0.1912$. The excellent agreement is found in two results. It is validated that the present GKUA can be commendably applied to solve unsteady continuum flow in diatomic gas.

Time-variation processes of density distribution in the shock-tube flow with different Kn numbers of $Kn=0.0001,0.01,0.1,1$ are described in Figs. 4(a)-(d). From the initial time $t=0$, the gas flow at two sides of diaphragm begins to interact due to the difference of initial states for density and temperature. Gas moves from high density area ($x<0.5$) to low density area ($x>0.5$). For the continuum ($Kn=0.0001$) and near-continuum ($Kn=0.01$) flows shown in Figs. 4(a) and (b), the expanding wave appears and moves to the left side of the diaphragm, and the shockwave emerges and spreads to the right side due to the gas compression. For the transitional flow regime of $Kn=0.1$ and high rarefied regime of $Kn=1$ shown in Figs. 4(c) and (d), there is no shock and expanding wave, but strong disturbance with compression and expansion exists and spreads to right

https://doi.org/10.4208/aamm.2014.m523 Published online by Cambridge University Press

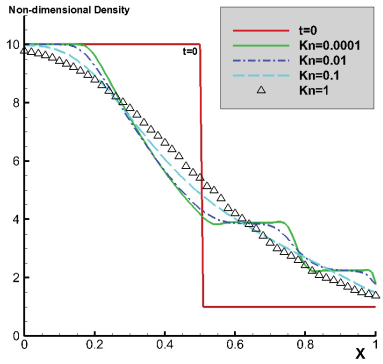


Figure 5: Comparison of density distribution for various Kn when $t=0.3$.

and left, respectively. It is indicated from density profiles at different time from $t=0$ to $t=0.3$ that the two-types of flow gradually spread to the both ends in an unsteady varying process. The spreading velocity of disturbance for the rarefied flow of $Kn=0.1$ and $Kn=1$ is not equal to the propulsive velocity of shockwave and expanding wave for the near-continuum of $Kn=0.01$ and continuum flow of $Kn=0.0001$. The front shown in Figs. 4(c) and (d) may move faster than the second shown in Figs. 4(a) and (b). This is identical to the spreading theory of wave and disturbance that wave shoves flow in continuum regime and disturbance spread as velocity of sound. It is also shown from Fig. 4 that rarefied gas effect becomes more severe, and shockwave and expanding wave are weakened and degenerated as Kn number increases. This transport characteristics can be clearly shown in Fig. 5, where the comparison of density distributions is given for different Kn numbers at $t=0.3$, and the strong disturbance has spread out the shock-tube when the shockwave of continuum flow arrives at the end of the shock-tube.

3.2 Numerical validation of unsteady two-dimensional planar jet flow in highly rarefied free-molecular flow regime

In [48], an analytical solutions of highly rarefied free molecular jet expanding into a vacuum from a exit has been developed and applied to study the two-dimensional planar jet flows depicted in Fig. 6, where the flow studied is a free molecular gas leaving a planar exit into a vacuum with $H=0.5$m and the non-dimensional velocity $S_0=2$. The gas at the exit is in an equilibrium state with a Maxwellian distribution. Here, in order to validate the direct Boltzmann gas-kinetic solver, this problem is numerically solved by the present GKUA, where the kinetic model is set as the collisionless Boltzmann equation, and only convection terms are considered as follows,

$$\frac{\partial f}{\partial t}+\xi_x\cdot\frac{\partial f}{\partial x}+\xi_y\cdot\frac{\partial f}{\partial y}=0. \tag{3.1}$$

The unsteady flow course is simulated from starting up to steady state. We capture the jet starting up at the moment of $t/T_*=1.0$, where $T_*=H/\sqrt{2RT_0}$. Fig. 7 shows

https://doi.org/10.4208/aamm.2014.m523 Published online by Cambridge University Press

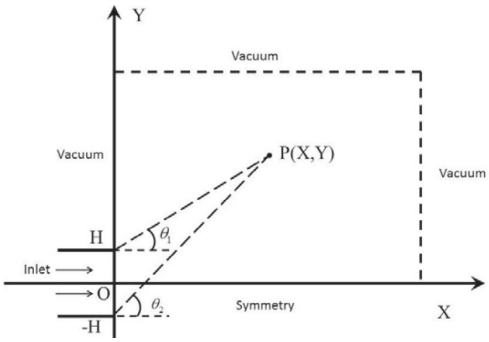
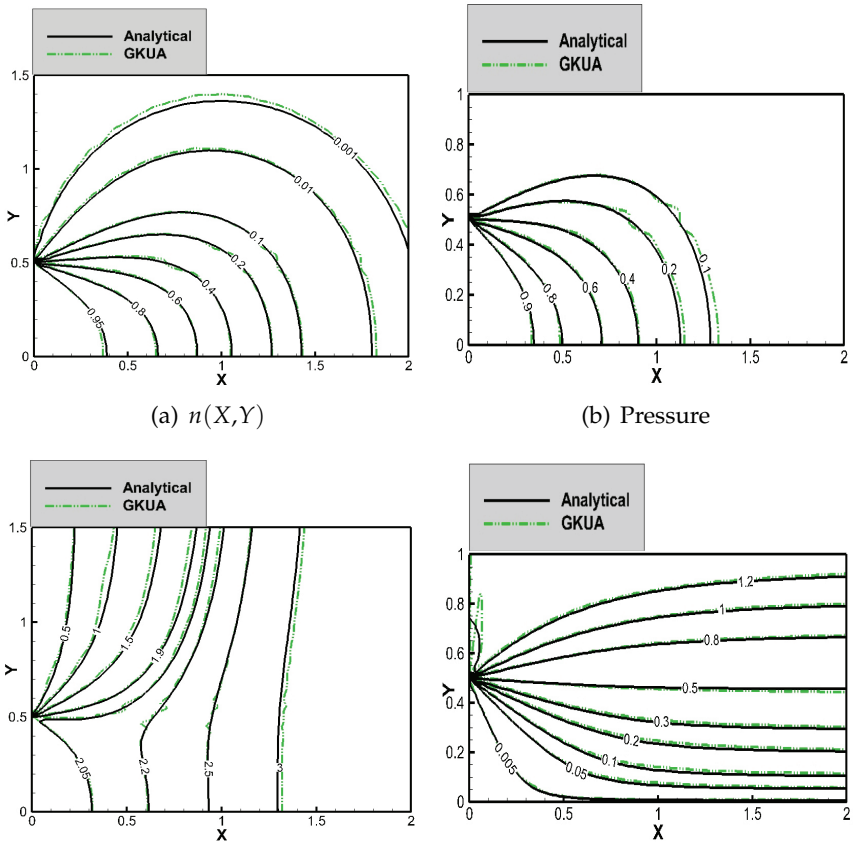


Figure 6: Illustration for the two-dimensional problem of planar jet flow into a vacuum.



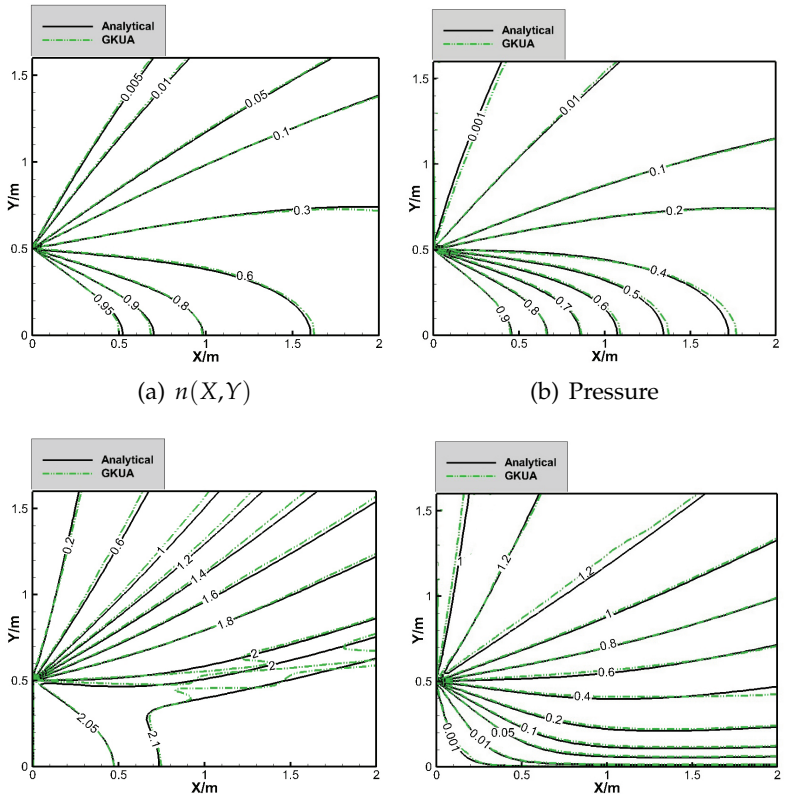
(a) $n(X,Y)$ (b) Pressure

(c) X-momentum (d) Y-momentum

Figure 7: Flow field distribution contours for planar jet flow in the startup process at time $t/T_* = 1.0$.

the comparison of non-dimensional flow parameters including the computed contours (dashed line) of number density, pressure, momentum components of $X-$ and $Y-$ directions with the analytical results from [48] (solid line). Overall, The GKUA results and the

https://doi.org/10.4208/aamm.2014.m523 Published online by Cambridge University Press



(a) $n(X,Y)$ (b) Pressure

(c) X-momentum (d) Y-momentum

Figure 8: Flow field distribution contours for planar jet flow in the steady state.

analytical solutions have good agreement in the startup process at time $t/T_* = 1.0$.

The high-speed jet expands into vacuum, and finally a steady flow field is set up as time goes by. Fig. 8 gives the steady-state macroscopic variables contours for the planar jet flow. In general, the GKUA results and the analytical solutions have essentially identical agreement in the flow field of the physical space (X,Y). It is shown that the plume expands quickly into vacuum and the exit lip is a singularity point with very large gradients. Because the effect of molecular collisions is neglected, all particles from the jet exit move forward, and no negative U-velocity component is observed. Gas diffusion is due to slow particles moving from the exit rather than intermolecular collisions. Inside the plume core, the forward moving particles dominate because of the high exit velocity. Along the vertical line above the exit, density and U-velocity almost approach to zero because no particles can reach there without intermolecular collisions. It is indicated from Figs. 7 and 8 that the unsteady varying course of two-dimensional planar jet flow is revealed from starting up to steady flow state, and the analytical method [48] based on the theory of free molecular flow is more economic with an approximate treatment on complete Maxwellian equilibrium distribution, but is limited in some special geometry

https://doi.org/10.4208/aamm.2014.m523 Published online by Cambridge University Press

and flow reduction, while the present GKUA can be applied to the flow around arbitrary geometric body but costly.

3.3 Simulation of unsteady flow in slip transitional flow regime through a slit

The gas flow through a slit into vacuum or at arbitrary pressure ratio is a fundamental problem as a benchmark to test numerical methods for the unsteady rarefied gas flows. Fig. 9 shows the illustration of the two-dimensional flow with two reservoirs at different pressures characterized by two parameters [47]: rarefaction parameter κ and pressure ratio p_1/p_0. The flow in the left high-pressure reservoir with p_0 and T_0 at initial time $t=0$ goes into the right low-pressure reservoir with p_1 and T_0, and the flow approaches to a steady state by an unsteady varying process.

$$\kappa=\frac{p_0 H}{\mu_0 s_0}, \quad s_0=\sqrt{2RT_0}. \tag{3.2}$$

Thus

$$Kn\propto\frac{1}{\kappa}. \tag{3.3}$$

This problem is solved by the present GKUA on the basis of the unsteady S-model for two cases of the rarefaction parameter $\kappa=10$ and the pressure ratios $p_1/p_0=0.5$,0.1, respectively, where the $\kappa=10$ corresponds to a near-continuum slip transitional flow regime. Figs. 10 and 11 show the time evolution of macroscopic flow variables including number density, flow velocity in X- direction and temperature along the symmetry axis ($y=0$). The computed distribution of the transient gas flow at arbitrary time $t=0.4\sim$ 18 from the GKUA are in good agreement with the results from [47] for the different pressure ratios of $p_1/p_0=0.5$ and 0.1. It is indicated from Figs. 10 and 11 that the gas flow varies with a unsteady perturbing process of the gas expansion into vacuum, and the macroscopic flow profiles mostly tend and get to the steady state as time elapses for $t\sim18$. The initial disturbances become stronger when the pressure ratio decreases and the flow approaches to vacuum in the right reservoir of the slit, especially for the flow velocity

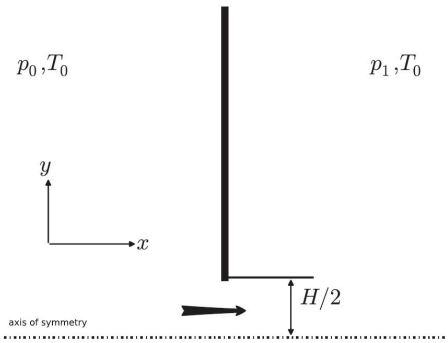


Figure 9: A sketch of the flow and coordinates with two reservoirs at different pressures.

https://doi.org/10.4208/aamm.2014.m523 Published online by Cambridge University Press

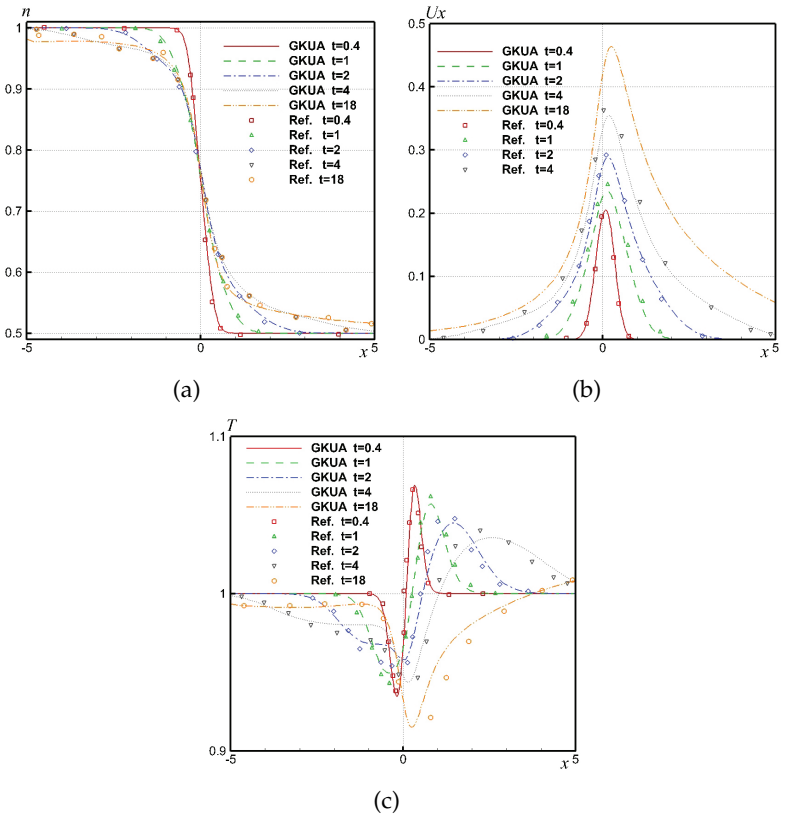


Figure 10: The evolution of macroscopic parameters in time, $\kappa=10$, $p_1/p_0=0.5$.

and the temperature shown in Fig. 11, and then, the longer time seems to be needed to reach the steady state through the slit. These initial disturbances diffuse in the whole computational domain due to the movement and collision of molecules, in particular, the flow compression from the left high-pressure reservoir to the right low-pressure reservoir through the slit leads to visible jump of temperature profile. By contrary, the flow profiles of number density, macroscopic velocity and temperature in the left reservoir deviate slightly and approach to smooth and steady distribution up to $x=-5$ from the slit.

3.4 Interaction of normal shock with detached shock in continuum and near-continuum transitional flow regimes

As examples of application of unsteady flows covering various flow regimes, the unsteady varying process for the gas flows of shockwave perturbation motion and interaction past a circular cylinder is solved with different Knudsen numbers of $0.0001\leq Kn\leq 1$ in nitrogen. The newly developed GKUA is applied by the use of the R-model involving the effect of rotational energy with 81×51 of the grid division in physical space, where the rotational characteristic parameter is set as $B=0.5553$ corresponding to reference tem-

https://doi.org/10.4208/aamm.2014.m523 Published online by Cambridge University Press

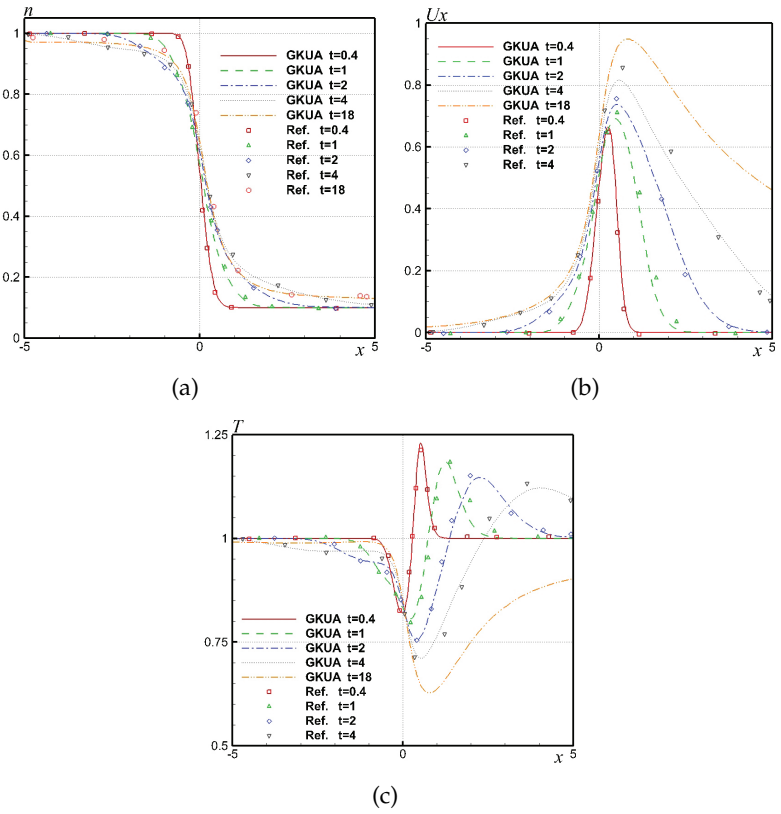


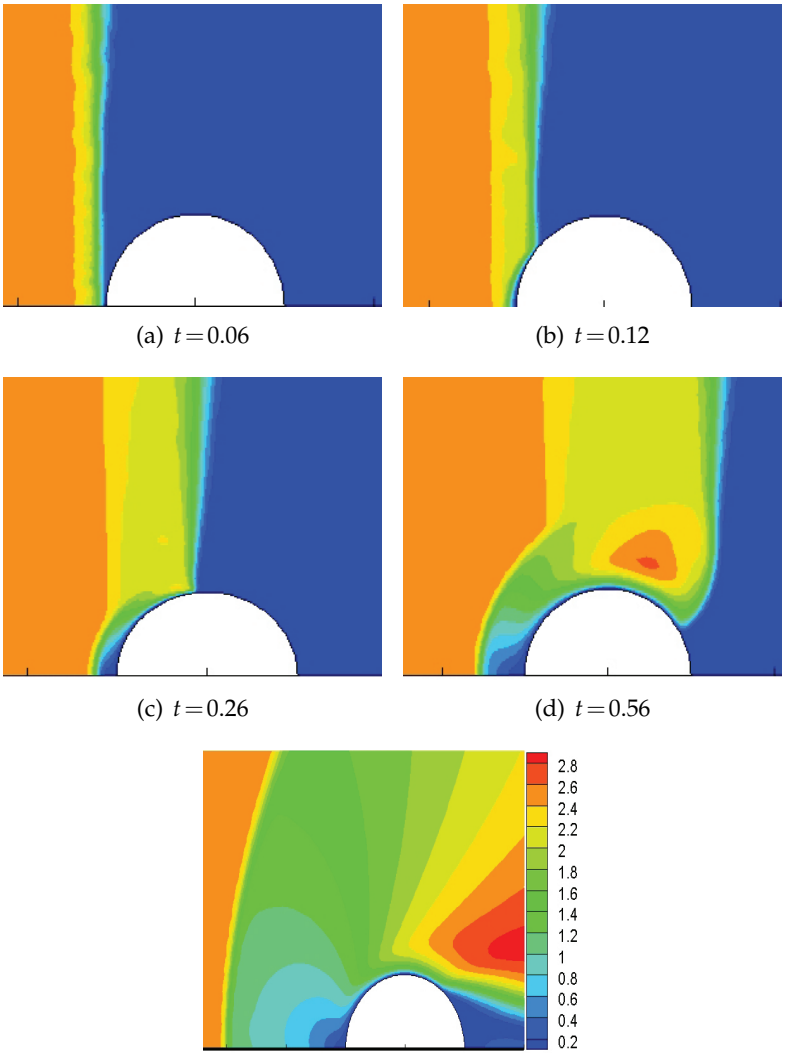
Figure 11: The evolution of macroscopic parameters in time, $\kappa=10$, $p_1/p_0=1$.

perature $T_\infty=50.81K$ and wall temperature $T_w=76.2K$ with specific heat ratio $\gamma=1.4$. The radius of the cylinder is 0.5. Initially, the gas flow velocity around the cylinder is zero, and an incident shock with Mach number 2.5 is arbitrarily located at a certain distance to the left of the cylinder as initial position, that is $x=-0.7$, where the origin is in the center of cylinder. This shockwave moves rightwards and interacts with the cylinder.

Fig. 12 shows the unsteady shock wave diffraction process for the shockwave movement and interaction with cylinder with $Kn=0.005$ in near-continuum regime, in which Mach number contours are shown at different time $t=0.06$,0.12,0.26,0.56 and 10. The plane moving shock wave impinges upon the circular cylinder as the beginning time at $t=0.06$, and leaves at $t=0.56$. Then this shockwave continually moves right towards far field. Regions ahead of the shockwave are quiescent and undisturbed. The gas flow behind the moving shockwave is affected and disturbed, and then gradually tends to new equilibrium flow state.

To reveal this unsteady varying process in a rarefied gas flow, Fig. 13 shows the strong discontinuous perturbation motion around the cylinder with $Kn=0.3$ in transitional regime. Some same flow characters are shown with quiescent flow ahead of the incident shock disturbance, and the disturbed gas flow trend to new equilibrium state

https://doi.org/10.4208/aamm.2014.m523 Published online by Cambridge University Press



(a) $t=0.06$ (b) $t=0.12$

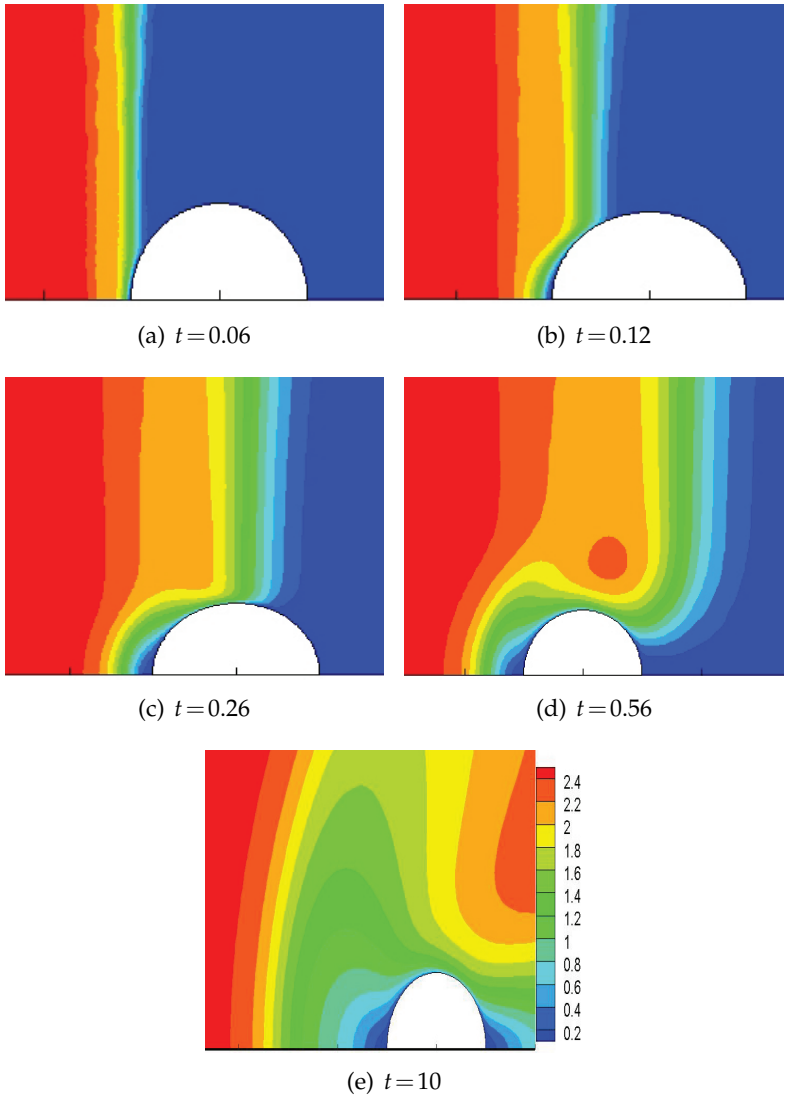
(c) $t=0.26$ (d) $t=0.56$

(e) $t=10$

Figure 12: Unsteady shock $M_s=2.5$ diffraction around a circular cylinder for the near-continuum flow of $Kn=0.005$.

behind the shock perturbation motion as in Fig. 12. Nevertheless, there are great differences from flows in continuum and rarefied transitional regimes by comparing Fig. 12 with Fig. 13. For the near-continuum flow of $Kn=0.005$ shown in Fig. 12, the shape and character of the incident shock can be preserved all along while the shockwave moves rightward until the discontinuity breaks in beyond distance, and the new bow shockwave that appears at a certain distance in the left side of cylinder is still strong bow wave as the incident shock. However, for the rarefied transitional flow of $Kn=0.3$ shown in Fig. 13, strong discontinuity of initial shockwave is set in the same way with Mach num-

https://doi.org/10.4208/aamm.2014.m523 Published online by Cambridge University Press



(a) $t=0.06$ (b) $t=0.12$

(c) $t=0.26$ (d) $t=0.56$

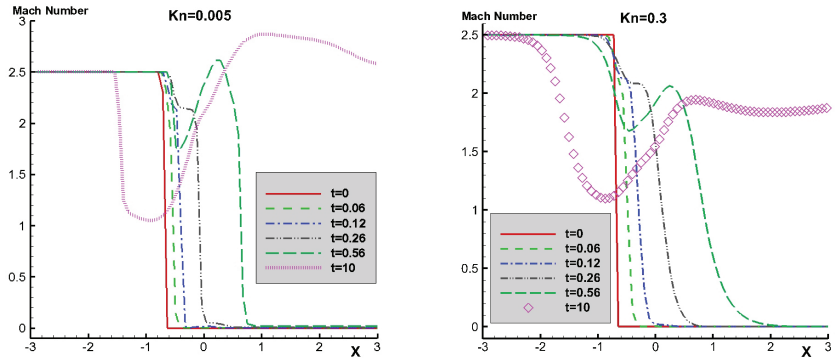
(e) $t=10$

Figure 13: Unsteady shock perturbation $(M_s=2.5)$ motion around a circular cylinder for the rarefied flow of $Kn=0.3$.

ber 2.5 and position $x=-0.7$, but the width of this shockwave disturbance increases as the perturbation motion goes ahead around the cylinder, and the discontinuity becomes faint. Only strong disturbance occurs at a farther distance in the left side of cylinder without bow shockwave after the unsteady perturbation motion passes by the cylinder and the flow approaches to tranquilization.

The varying course of Mach number distribution along with position x at $y=0.64$ is quantificationally shown in Fig. 14 for $Kn=0.005$ and 0.3, respectively. In Fig. 14(a), the movements of the incident shock at $t=0.06$,0.12 and 0.26, the formation of the bow shock

https://doi.org/10.4208/aamm.2014.m523 Published online by Cambridge University Press



(a) near-continuum regime with $Kn=0.005$

(b) Rarefied transitional regime with $Kn=0.3$

Figure 14: Time-variation process of Mach number distribution along with x at y=0.64 for different Kn numbers.

and oblique shock wave at $t=0.56$ and $t=10$ during the diffraction and interaction of the moving shock wave around the cylinder are obviously included for the near-continuum flow of $Kn=0.005$. In Fig. 14(b), the whole process of strong discontinuous perturbation motion around the cylinder is revealed and token at different time $t=0.06,0.12,0.26,0.56$ and 10 for the rarefied transitional flow of $Kn=0.3$. Especially, it is indicated that the range of disturbed effect for the rarefied flow of $Kn=0.3$ is bigger than that for the near-continuum flow of $Kn=0.005$ at each time, and the Mach number values in the downstream expanding region of the cylinder for continuum regime of $Kn=0.005$ exceed the incident shock Mach number behind the shock perturbation motion passes by the cylinder, however, the disturbed flow clings to the body surface without this expanding flow phenomena for the rarefied flow of $Kn=0.3$.

Finally, we study the interaction of a normal shock with a detached shock wave in continuum and near-continuum slip regimes, where the detached shock wave is formed at a certain distance to the left of the cylinder with free-stream Mach number of Ma_∞=1.6. When the gas flow is stable around the cylinder, another normal shockwave of $Ma_\infty=2.5$ is located ahead of the detached shockwave at the location $x=-2$ shown in Figs. 15(a) and 16(a). At the beginning, the detached shock is static and steady, while the normal shockwave moves rightward and then interact with the detached shock. The whole unsteady process is simulated by the GKUA for diatomic gases with different Knudsen numbers of $Kn=0.0001$ and $Kn=0.08$. Shown in the (a) to (i) of Figs. 15 and 16 are Mach number contours distribution at several different times for Kn=0.0001 and Kn=0.08, respectively. From the beginning in the (a) of the two Figs. 15 and 16, the normal shockwave moves and closes to the detached shock. To the moment in (b), the normal shockwave arrives at the location of the detached shock, these two shockwaves begin to combine and form an interaction-resulting Mach shockwave. This Mach shockwave begins to separate from (c) to (d), and finally forms two new individual shockwaves in (e). But it is obviously shown that intensity of the left derivative shockwave is weaker, and this shockwave s-

https://doi.org/10.4208/aamm.2014.m523 Published online by Cambridge University Press

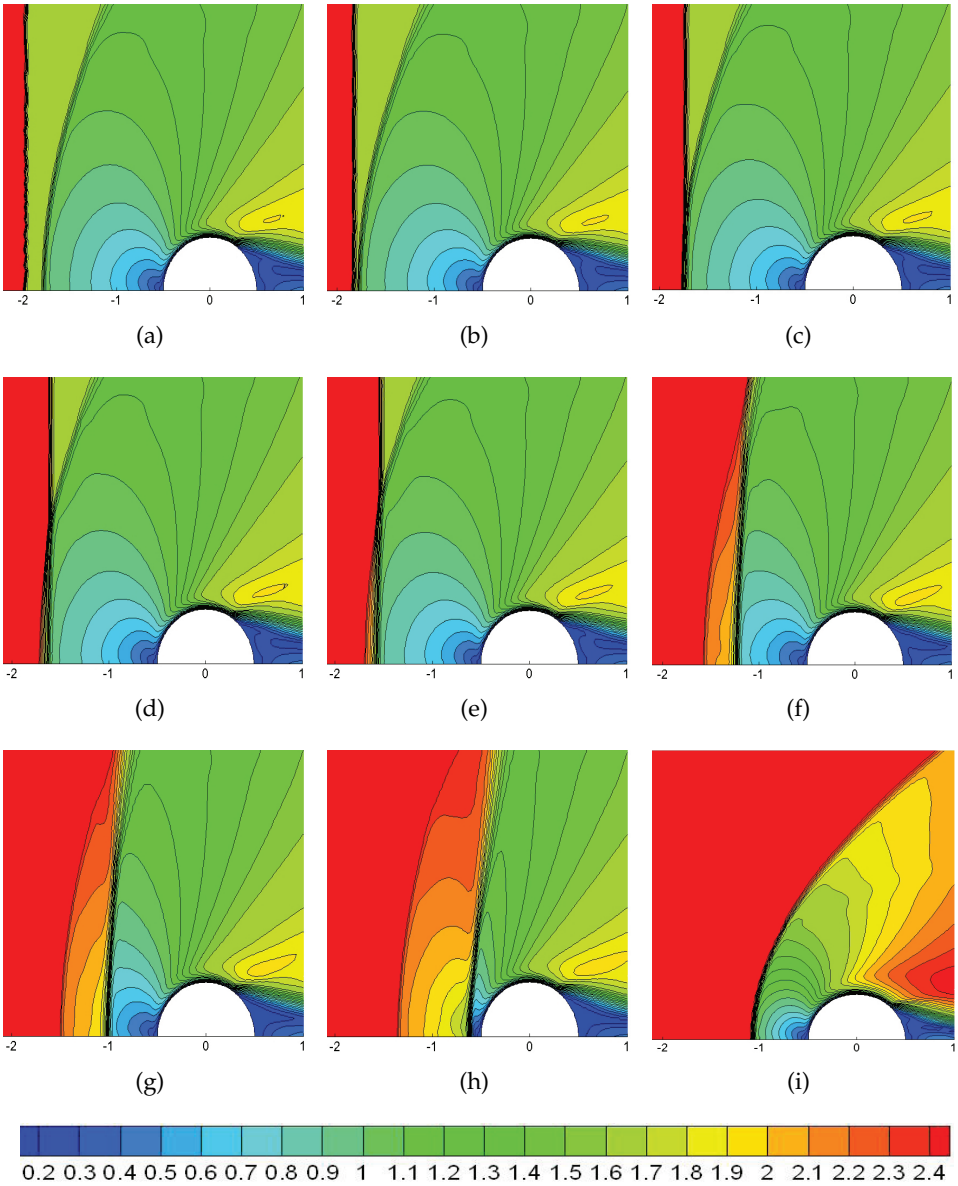


Figure 15: Mach number contours for the interaction of normal shock with detached shock wave in continuum flow of $Kn = 0.0001$.

lowly moves outwards due to the free streaming. The moving velocity of this shockwave is much less than the forward one. The stronger shockwave continuously runs rightward, interacts and impinge on the surface of the circular cylinder shown in (f). The reflected wave forms from impingement on the cylinder surface, and rebounds to move outwards, then converges with the forgoing derivative shockwave from (g) to (i). On the other hand, the interaction-attached shockwave around the cylinder moves rightward along,

https://doi.org/10.4208/aamm.2014.m523 Published online by Cambridge University Press

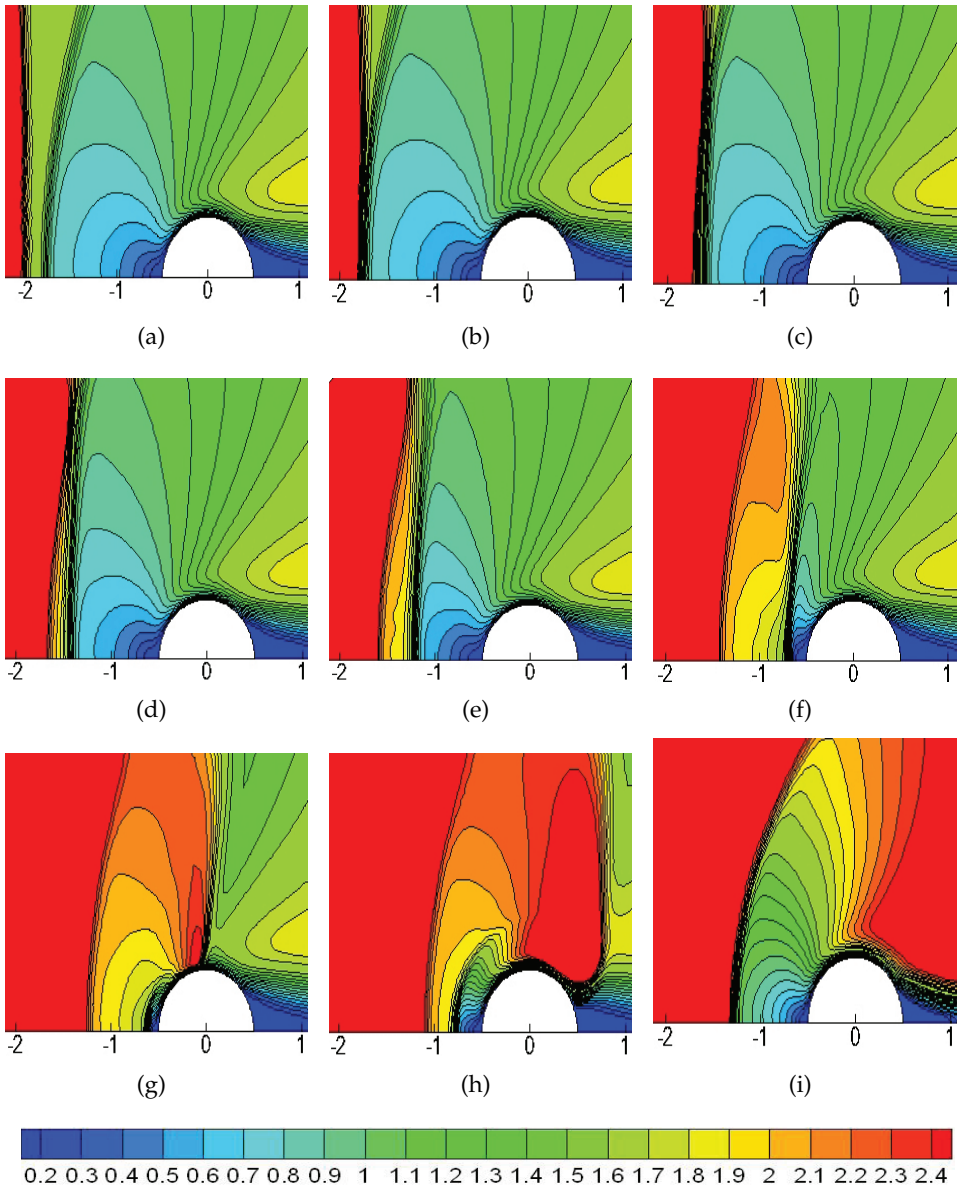


Figure 16: Mach number contours for interaction of normal shock with detached shock in near-continuum slip flow of $Kn = 0.08$.

arrives at the leeward area, and interacts with original compression wave and wake flow, which is shown from (g) to (i), respectively. Then, the compression wave in leeward area is strengthened. Finally, the flow field around the circular cylinder gets a new steady state, and a new stable detached shockwave gradually appears at a nearer distance than that of the original detached shock to the left of the cylinder shown in (i). The whole pro-

https://doi.org/10.4208/aamm.2014.m523 Published online by Cambridge University Press

cess looks like that the normal shockwave passes through the original detached shock. But actually, the character and intensity of these two shockwaves obviously change after interaction. The intensity of the derivative detached shock is greatly weakened by the interaction with the normal shockwave, and then strengthened by the reflected shock from cylinder surface. Consequently, the original detached shock is finally swallowed into a new and stronger detached shock wave, which can be well captured with the stagnation region, downstream wake, complicated flow interaction-resulting Mach shocks in (i).

It is also shown by comparing Fig. 15 and Fig. 16 that, although the interacting process of two shockwaves is completely similar both in Fig. 15 corresponding to the continuum regime for $Kn = 0.0001$ and in Fig. 16 related to the near-continuum slip regime for $Kn = 0.08$, the discontinuous features of shockwaves in the whole interacting process are more obvious and the shockwaves are more crisp and thin in the continuum flow case of $Kn = 0.0001$, and the thickening of the front bow shock is noticeable difference in the near-continuum slip flow of $Kn = 0.08$.

4 Conclusions

In this paper, the direct Boltzmann gas-kinetic solver for unsteady gas dynamics covering flow regimes has been developed by using the gas-kinetic unified algorithm (GKUA), where both the S-model for monatomic ideal gases and the R-model for diatomic gases involving the effect of rotational degrees of freedom are applied. To simplify and integrate the distribution function over the energy variable, the Rykov kinetic equation is integrated by the weight factor on the internal energy and transformed into two kinetic governing equations with inelastic and elastic collisions. Then, the reduced velocity distribution functions and the discrete velocity ordinate (DVO) method are applied to develop the computable hyperbolic conservation model, and the time-explicit finite-difference scheme and numerical stability condition to fix on the time step are devised by the aid of the unsteady operator-splitting technique to numerically solve the reduced velocity distribution functions at each of DVO point.

In the second part of this paper, the newly developed GKUA is applied to study the unsteady one- and two-dimensional flows from continuum to rarefied transitional flow regimes. The unsteady flow solver is validated to simulate the one-dimensional unsteady shock-tube problem in continuum regime and the unsteady two-dimensional planar jet flow and the gas flow through a slit in rarefied transitional flow regime by the use of S-model, where the simulation results match the analytical solutions and typical reference data accurately. Then, the time-variation processes including the unsteady shock-tube flow and the interaction of normal shock with detached shock around a circular cylinder is solved by using the Boltzmann-Rykov model equation involving in the effect of rotational energy in diatomic gases with $10^{-1} \leq Kn \leq 1$, where some significative flow phenomena and unsteady flow mechanism are revealed and analyzed. It can be tasted from this study that the present gas-kinetic numerical algorithm provides an important and

https://doi.org/10.4208/aamm.2014.m523 Published online by Cambridge University Press

feasible tool to solve the unsteady gas flow problems covering various flow regimes. Further investigations on the kinetic models for multi-component real gas non-equilibrium effects involving internal energy excitation and the three-dimensional complex unsteady flows et al., need to be studied in the future.

Acknowledgments

This work was supported by the National Key Basic Research and Development Program (2014CB744100) and the National Nature Science Foundation of China under Grant Nos. 91016027 and 11325212.

References

[1] H. Bergh, H. Tijdeman and R. J. Zwaan, Theory and Experiment in Unsteady Aerodynamics, Aeroelastic Colloquium, Gottingen, N82-17128, 1980.
[2] A. R. D. Thorley and C. H. Tiley, *Unsteady and transient flow of compressible fluids in pipelinesła review of theoretical and some experimental studies,* Int. J. Heat Fluid Flow, 8 (1987), pp. 3–15.
[3] A. El Chebair, A. K. Misra and M. P. Paidoussis, *Theoretical study of the effect of unsteady viscous forces on inner- and annular-flow-induced instabilities of cylindrical shells,* J. Sound Vibration, 138 (1990), pp. 457–478.
[4] A. Azuma and M. Okamoto, *Theoretical study on two-dimensional aerodynamic characteristics of unsteady wings,* J. Theoretical Biology, 234 (2005), pp. 67–78.
[5] Z. Jiang, K. Takayama, H. Babinsky and T. Meguro, *Transient shock wave flows in tubes with a sudden change in cross section,* Shock Waves, 7 (1997), pp. 151–162.
[6] J. D. H. Kelder, R. J. H. Dijkers, B. P. M. Esch and N. P. Kruyt, *Experimental and theoretical study of the flow in the volute of a low specific-speed pump,* Fluid Dynamics Research, 28 (2001), pp. 267–280.
[7] M. Mamou, A. Tahi, A. Benmeddour, K. R. Cooper, I. Abdallah, M. Khalid and J. Fitzsimmons, *Computational fluid dynamics simulations and wind tunnel measurements of unsteady wind loads on a scaled model of a very large optical telescope: A comparative study,* J. Wind Eng. Indust. Aerodyn., 96 (2008), pp. 257–288.
[8] E. C. Mladin and J. Padet, *Unsteady planar stagnation flow on a heated plate,* Int. J. Thermal Sci., 40 (2001), pp. 638–648.
[9] R. M. Fernie and H. Babinsky, *Unsteady shock motion on a NACA0012 aerofoil at low reduced frequencies,* AIAA, 2004-49.
[10] Jeffrey P. Thomas and Chad H. Custer, *Unsteady flow computation using a harmonic balance approach implemented about the overflow2 flow solver,* AIAA, 2009-4270.
[11] Q. M. Al-Mdallal, *A numerical study of initial flow past a circular cylinder with combined streamwise and transverse oscillations,* Comput. Fluids, 63 (2012), pp. 174–183.
[12] T. Ohwada, Y. Sone and K. Aoki, *Numerical analysis of the shear and thermal creep flows of a rarefied gas over a plane wall on the basis of the linearized Boltzmann equation for hard-sphere molecules,* Phys. Fluids A, 1 (1989), pp. 1588–1599.
[13] J. V. Austin and D. B. Goldstein, *Rarefied gas model of Io's sublimation-driven atmosphere,* Icarus, 148 (2000), pp. 370–383.

https://doi.org/10.4208/aamm.2014.m523 Published online by Cambridge University Press

[14] S. APTE AND V. YANG, *Unsteady flow evolution and combustion dynamics of homogeneous solid propellant in a rocket motor,* Combus. Flame, 131 (2002), pp. 110–131.
[15] G. A. BIRD, *Approach to translational equilibrium in a rigid sphere gas,* Phys. Fluids, 6 (1963), pp. 1518–1519.
[16] G. A. BIRD, Molecular Gas Dynamics and the Direct Simulation of Gas Flows, Oxford University Press, 1994.
[17] Z. L. LI, J. LIANG AND Y. R. XIE, *DSMC analysis of normal shock wave structure in gas mixtures involving internal energy transfer,* Proc. Second ASIA Workshop on Computational Fluid Dynamics, Tokyo, Japan, December 19-23, (1996), pp. 233–238.
[18] A. A. ALEXEENKO, D. A. FEDOSOV, S. F. GIMELSHEIN AND D. A. LEVIN, *Transient heat transfer and gas flow in a MEMS-based thruster,* J. Microelectromech. Syst., 15 (2006), pp. 181–194.
[19] MARK GOLDSWORTHY, MICHAEL MACROSSAN AND MADHAT ABDEL-JAWAD, *Simulation of unsteady flows by the DSMC macroscopic chemistry method,* J. Comput. Phys., 228 (2009), pp. 976–982.
[20] C. W. LIM, M. R. SMITH, H. M. CAVE, M. C. JERMY, J. S. WU AND S. P. KRUMDIECK, *The direction decoupled quiet direct simulation method for rapid simulation of axisymmetric inviscid unsteady flow in pulsed pressure chemical vapour deposition,* Comput. Fluids, 86 (2013), pp. 14–27.
[21] FELIX SHARIPOV, *Transient flow of rarefied gas through a short tube,* Vacuum, 90 (2013), pp. 25–30.
[22] YOUNG-KYU HWANG, JOONG-SIK HEO AND MYOUNG-KEUN KWON, *Unsteady computations of rarefied gas flows induced by a rotor-stator interaction in a disk-type drag pump,* Rarefied Gas Dynamics, 23rd International Symposium, 2003.
[23] N. HADJICONSTANTINOU, A. GARCIA, M. BAZANT AND G. HE, *Statistical error in particle simulations of hydrodynamic phenomena,* J. Comput. Phys., 187 (2003), pp. 274–297.
[24] SRUTI CHIGULLAPALLI AND ALINA ALEXEENKO, *Unsteady 3D rarefied flow solver based on Boltzmann-ESBGK model kinetic equations,* AIAA, 2011-3993.
[25] C. CERCIGNANI, Kinetic Theories and the Boltzmann Equation, Lecture Notes in Mathematics, Springer-Verlag, Berlin, 1984.
[26] L. S. LUO, M. KRAFCZYK AND Y. LIU, *Mesoscopic methods in engineering and science,* Int. Comput. Fluid Dyn., 20 (2006), pp. 359–360.
[27] Z. H. LI AND H. X. ZHANG H X, *Gas-kinetic numerical method solving mesoscopic velocity distribution function equation,* Acta Mech. Sinica, 23 (2007), pp. 21–132.
[28] L. MIEUSSENS, *Discrete velocity model and implicit scheme for the bgk equation of rarefied gas dynamics,* Math. Models Meth. Appl. Sci., (2000).
[29] ALEXANDER WAGNER, Theory and Applications of the Lattice Boltzmann Method, University of Oxford, 1997.
[30] JAMES MAXWELL BUICK, Lattice Boltzmann Methods in Interfacial Wave Modelling, Philosophy: The University of Edinburgh, 1997.
[31] X. NIE, G. D. DOOLEN AND S. CHEN, *Lattice Boltzmann simulation of fluid flows in MEMS,* J. Statist. Phys., 107 (2002), 279.
[32] DENIS RICOT, VIRGINIE MAILLARD AND CHRISTOPHE BAILLY, *Numerical simulation of unsteady cavity flow using lattice Boltzmann method,* AIAA, 2002-2532.
[33] K. XU, *A gas-kinetic BGK scheme for the Navier-Stokes equations and its connection with artificial dissipation and Godunov method,* J. Comput. Phys., 171 (2001), pp. 289–335.
[34] K. XU AND Z. H. LI, *Microchannel flow in the slip regime: gas-kinetic BGK-Burnett solutions,* J.

https://doi.org/10.4208/aamm.2014.m523 Published online by Cambridge University Press

Fluid Mech., 513 (2004), pp. 87–110
[35] Z. H. Li and H. X. Zhang, *Study on gas kinetic unified algorithm for flows from rarefied transition to continuum,* J. Comput. Phys., 193 (2004), pp. 708–738.
[36] S. Z. Chen, K. Xu, C. B. Lee and Q. D. Cai, *A unified gas kinetic scheme with moving mesh and velocity space adaptation,* J. Comput. Phys., 231 (2012), pp. 6643–6664.
[37] Z. L. Guo and C. G. Zheng, Theory and Applications of Lattice Boltzmann Method, Beijing: Science Press, 2009.
[38] H. B. Huang, X. Y. Lu and M. Krafczyk, *Numerical simulation of unsteady flows in Czochralski crystal growth by lattice Boltzmann methods,* Int. J. Heat Mass Trans., 74 (2014), pp. 156–163.
[39] K. Hejranfar and E. Ezzatneshan, *Implementation of a high-order compact finite-difference lattice Boltzmann method in generalized curvilinear coordinates,* J. Comput. Phys., 267 (2014), pp. 28–49.
[40] P. L. Bhatnagar, E. P. Gross and M. Krook, *A model for collision processes in gases: i. small amplitude processes in charged and neutral one-component systems,* Phys. Rev., 94 (1954), pp. 511–525.
[41] Jr. L. H. Holway, *New statistical models for kinetic theory: methods of construction,* Phys. Fluids, 9 (1966), pp. 1658–1673.
[42] E. M. Shakhov, *Generalization of the krook kinetic relaxation equation,* Fluid Dyn., 3 (1968), pp. 142–145.
[43] Z. H. Li and H. X. Zhang, *Gas-kinetic description of shock wave structures by Boltzmann model equation,* Int. J. Comput. Fluid Dyn., 22 (2008), pp. 623–638.
[44] Christopher D. Wilson and R. K. Agarwal, *Computation of hypersonic flow of a diatomic gas in rotational nonequilibrium past 3d blunt bodies using the generalized Boltzmann equation,* AIAA, 2009-3836.
[45] John Lihnaropoulos and Dimitris Valougeorgis, *Unsteady vacuum gas flow in cylindrical tubes,* Fusion Eng. Design., 86 (2011), pp. 2139–2142.
[46] Sruti Chigullapalli and Alina Alexeenko, *Unsteady 3D rarefied flow solver based on Boltzmann-ESBGK model kinetic equations*, AIAA, 2011-3993.
[47] A. Ph. Polikarpov and I. Graur, *Unsteady rarefied gas flow through a slit,* Vacuum, 101 (2014), pp. 79–85.
[48] Chunpei Cai and L. Wang, *Gas kinetic analytical and numerical studies on rarefied unsteady planar jet flows,* Phys. Scripta, 88 (2013), pp. 1–8.
[49] C. Cai, Q. Sun and A. Vanderwyst, *Analytical exact solutions for unsteady collisionless plume flows in a vacuum,* Acta Astronautica, 91 (2013), pp. 218–227.
[50] Z. H. Li, Study on Gas-Kinetic Unified Algorithm from Rarefied Transition to Continuum, Mianyang in Sichuan: China Aerodynamics Research and Development Center, 2001.
[51] Z. H. Li and H. X. Zhang, *Numerical investigation from rarefied flow to continuum by solving the Boltzmann model equation,* Int. J. Numer. Methods Fluids, 42 (2003), pp. 361–382.
[52] Z. H. Li and H. X. Zhang, *A gas kinetic algorithm for flows in microchannel,* Int. J. Nonlinear Sci. Numer. Simulation, 6 (2005), pp. 261–270.
[53] Z. H. Li and H. X. Zhang, *Gas-kinetic numerical studies of three-dimensional complex flows on spacecraft re-entry,* J. Comput. Phys., 228 (2009), pp. 1116–1138.
[54] V. A. Rykov, *Model kinetic equation of a gas with rotational degrees of freedom,* Fluid Dyn., 10 (1975), pp. 959–966.
[55] E. M. Shakhov, *Approximate kinetic equations in rarefied gas theory,* Fluid Dyn., 3 (1968), pp. 156–161.

https://doi.org/10.4208/aamm.2014.m523 Published online by Cambridge University Press

[56] V. A. RYKOV, V. A. TITAREV AND E. M. SHAKHOV, *Numerical study of the transverse supersonic flow of a diatomic rarefied gas past a plate,* Comput. Math. Math. Phys., 47 (2007), pp. 136–150.
[57] V. A. RYKOV, V. A. TITAREV AND E. M. SHAKHOV, *Shock wave structure in a diatomic gas based on a kinetic model,* Fluid Dyn., 43 (2008), pp. 316–326.
[58] HANXIN ZHANG, *Numerical problems for unsteady flows,* 6th Countrywide Hydrodynamics Conference, Shanghai, 2001, 23-31.
[59] HANXIN ZHANG AND MENGYU SHEN, Computational Fluid Dynamics-Fundamentals and Applications of Finite Difference Methods, BeijingNational Defence Industry Press, 2003.
[60] Z. H. LI, M. FANG, X. Y. JIANG AND J. C. WU, *Convergence proof of the DSMC method and the gas-kinetic unified algorithm for the Boltzmann equation,* Sci. China Phys. Mech. Astronomy, 56 (2013), pp. 404–417.
[61] J. Y. YANG, *Rarefied flow computations using nonlinear model Boltzmann equations,* J. Comput. Phys., 120 (1995), pp. 323–339.
[62] J. Y. YANG AND J. C. HUANG, *Computations of kinetic model equations for gases with internal degrees of freedom,* AIAA, 95-2315.
[63] J. Y. YANG AND J. C. HUANG, *High resolution schemes for rarefied gas dynamics using kinetic model equations,* AIAA, 95-1678-CP.
[64] J. Y. YANG, *Nonoscillatory schemes for kinetic model equations for gases with internal energy states,* AIAA J., 34 (1996).

https://doi.org/10.4208/aamm.2014.m523 Published online by Cambridge University Press